FEBS Open Bio 2 (2012) 159–172

FEBS openbio

journal homepage: www.elsevier.com/locate/febsopenbio

The complex structures of isocitrate dehydrogenase from *Clostridium thermocellum* and *Desulfotalea psychrophila* suggest a new active site locking mechanism

Hanna-Kirsti S. Leiros [a,*], Anita-Elin Fedøy [b], Ingar Leiros [a], Ida Helene Steen [b,c]

[a] The Norwegian Structural Biology Centre (NorStruct), Department of Chemistry, University of Tromsø, N-9037 Tromsø, Norway
[b] Department of Biology, University of Bergen, P.O. Box 7803, N-5020 Bergen, Norway
[c] Centre for Geobiology, University of Bergen, P.O. Box 7803, N-5020 Bergen, Norway

ARTICLE INFO

Article history:
Received 2 May 2012
Revised 28 June 2012
Accepted 28 June 2012

Keywords:
Temperature adaptation
Thermophilic
Psychrophilic
NADP$^+$ selectivity
Domain movement

ABSTRACT

Isocitrate dehydrogenase (IDH) catalyzes the oxidative NAD(P)$^+$-dependent decarboxylation of isocitrate into α-ketoglutarate and CO_2 and is present in organisms spanning the biological range of temperature. We have solved two crystal structures of the thermophilic *Clostridium thermocellum* IDH (*Ct*IDH), a native open apo *Ct*IDH to 2.35 Å and a quaternary complex of *Ct*IDH with NADP$^+$, isocitrate and Mg^{2+} to 2.5 Å. To compare to these a quaternary complex structure of the psychrophilic *Desulfotalea psychrophila* IDH (*Dp*IDH) was also resolved to 1.93 Å. *Ct*IDH and *Dp*IDH showed similar global thermal stabilities with melting temperatures of 67.9 and 66.9 °C, respectively. *Ct*IDH represents a typical thermophilic enzyme, with a large number of ionic interactions and hydrogen bonds per residue combined with stabilization of the N and C termini. *Ct*IDH had a higher activity temperature optimum, and showed greater affinity for the substrates with an active site that was less thermolabile compared to *Dp*IDH. The uncompensated negative surface charge and the enlarged methionine cluster in the hinge region both of which are important for cold activity in *Dp*IDH, were absent in *Ct*IDH. These structural comparisons revealed that prokaryotic IDHs in subfamily II have a unique locking mechanism involving Arg310, Asp251′ and Arg255 (*Ct*IDH). These interactions lock the large domain to the small domain and direct NADP$^+$ into the correct orientation, which together are important for NADP$^+$ selectivity.

1. Introduction

Isocitrate dehydrogenase (IDH) is an enzyme in the tricarboxylic acid cycle, which catalyzes the oxidative NAD(P)$^+$-dependent dehydrogenation and decarboxylation of isocitrate to α-ketoglutarate and CO_2. IDH has a critical metabolic function and consequently is found in organisms from all domains of life. This enzyme has been extensively studied both kinetically and structurally from psychrophilic, mesophilic and (hyper)thermophilic organisms [1–19]. With respect to cofactor specificity and oligometric states the IDH enzyme represents a diverse family which is divided into three subfamilies based on the primary sequences [15]. Subfamiliy I includes archaeal and some bacterial IDH's, whereas subfamily II contains eukaryotic and bacterial IDH's but is absent from the archea. The amino acid sequence identity between subfamilies I and II is low (<20%), however the three-dimensional structures have similar folds and the key catalytically residues are conserved. The active IDH enzymes are functional as homodimers in both subfamilies, each monomer consists of a small and large, clasp domains which link the two subunits together, and the active sites being situated in the clefts between a large and a small domain from opposing subunits.

The crystal structure of the group I IDH from *Escherichia coli* (*Ec*IDH) was the first to be determined, subsequently many other *Ec*IDH structures with different substrates and conformations were resolved; leading to detailed knowledge of its catalytic mechanism [2,7,20–25].

In our earlier work, we have solved the three-dimensional structure of IDH from three different hyperthermophiles; *Archaeoglobus fulgidus* (*Af*IDH) [18], *Aeropyrum pernix* (*Ap*IDH) [8] and *Thermotoga maritima* (*Tm*IDH) [9], searching for stabilizing interactions and explanations for the thermal stability of these enzymes. This was explained by enlarged ionic networks and an increased number of ion pairs in *Ap*IDH and *Tm*IDH, but *Af*IDH was more similar to the

Abbreviations: IDH, isocitrate dehydrogenase; *Ct*IDH, *Clostridium thermocellum* IDH; *Dp*IDH, *Desulfotalea psychrophila* IDH; *Ec*IDH, *Escherichia coli* IDH; *Tm*IDH, *Thermotoga maritima*; *Pc*IDH, porcine heart mitochondrial IDH; *Hc*IDH, human cytosolic IDH; *Sc*IDH, *Saccharomyces cerevesiae* mitochondrial IDH; *Dh*IDH, *Desulfitobacterium hafniense* IDH; DSC, differential scanning calorimetry; T_m, apparent melting temperature

* Corresponding author. Fax: +47 77 64 47 65.
E-mail address: hanna-kirsti.leiros@chem.uit.no (H.-K.S. Leiros).

2211-5463 © 2012 Federation of European Biochemical Societies. Published by Elsevier B.V. Open access under CC BY-NC-ND license.
http://dx.doi.org/10.1016/j.fob.2012.06.003

mesophilic *Ec*IDH. All of the hyperthermophilic IDHs had stabilization of the N terminus; *Ap*IDH by a disulfide bond, *Tm*IDH by long-range electrostatic interactions and *Af*IDH through an aromatic cluster. These stabilizing factors are typical for hyperthermophilic proteins together with; loop shortening, stronger inter-subunit interactions, increased number of hydrogen bonds, a reduction of hydrophobic accessible surface area, increased number of ionic interactions at the surface and reduction of the repulsive charge–charge interactions [26,27,28,29]. An opposite trend is found for psycrophilic proteins, which are reported with an increase in surface charge, particularly a negative charge, an increase in hydrophobic accessible surface area, a reduced Arg/Lys ratio and higher methionine content [30,31]. However each stabilizing or destabilizing contribution is small and dependent on size, distance and position in the structure. As a result of this there is still no complete explanation of the activity–stability–flexibility relationship in cold adapted proteins.

In the search for cold-adaptive traits we performed a biochemical characterization and solved the crystal structure of IDH from the psychrophilic *Desulfotalea psychrophila* (*Dp*IDH), we found an enzyme with an unusual high thermal stability (T_m = 66.9 °C) and a moderate activity at its normal working temperature [4]. Its structure revealed stabilizing features such as; a unique ionic network in the clasp region, an aromatic cluster in the small domain, and multiple N- and C-termini ionic-interactions. This is counterbalanced by elements promoting flexibility such as a methionine cluster in the dimeric interface, destabilized negatively charged amino acids close to the active site and an acidic surface.

Structural analyses of *Saccharomyces cerevesiae* mitochondrial IDH (*Sc*IDH) one in an open conformation with $NADP^+$, two in quasi-closed conformations with isocitrate or α-ketoglutarate bound, and one fully closed quaternary complex with $NADP^+$, α-ketoglutarate and Ca^{2+}, representing different enzymatic states, have revealed fine-tuned conformational changes to occur during the catalytic reaction, compared to the *E. coli* IDH (*Ec*IDH) from subfamily I. Especially, the alpha helices α4 and α11, which are unique in the subfamily II enzymes, act as a lid covering the top of the $NADP^+$ and isocitrate-binding sites [32].

The availability of a range of three dimensional structures provided the opportunity to compare prokaryotic and eukaryotic IDHs within subfamily II. Therefore we have determined the crystal structure of IDH's from the thermophilic bacterium *Clostridium thermocellum*, the hyperthermophilic *T. maritima* (*Tm*IDH) [9], the psychrophilic *D. psychrophila* (*Dp*IDH) in both native and binary form with isocitrate [4], together these span a habitat temperature range from 0 to 80 °C.

We have expressed, characterized and crystallized *Ct*IDH, and obtained an open form (*Ct*IDH-Open) and a closed form of *Ct*IDH. The latter is a quaternary complex with $NADP^+$, isocitrate and a magnesium ion (*Ct*IDH–NADP). In addition, a structure of *Dp*IDH with $NADP^+$, isocitrate and Mg^{2+} (*Dp*IDH–NADP) was resolved and a comparative structural analysis was performed. These quaternary structures have displayed new interactions with the cofactor which lock the enzyme into a conformation ready for catalysis. Altogether, we now possess sufficient structures and in different states, open, closing, closed and locked, to suggest a new prokaryotic subfamily II IDH locking mechanism involved in substrate binding.

2. Materials and methods

2.1. Cloning, expression and purification

Putative *icd* genes from *C. thermocellum* (YP_001036717) and *D. psychrophila* (YP_064514), were amplified from genomic DNA by PCR using the following primer sets; 5′-CACCATGAGTAAGATAAAATGAAAGTTCCGTT-3′, 5′-TTATGCCATACCTTCAAAAGTTTTCCTG-3′ and 5′-GGGAATTCCATATGAAGATACAAATGAAAACTCCACTCG-3′, 5′-GCGGGATCCTTACTTGTTGAGCTGTTGCAATCTTTTGCC-3′.

The *Nde*I and *Bam*HI restriction sites are underlined. The cloning and purification of *Dp*IDH were performed as described earlier [4]. For the amplification of the *Ct*IDH gene the following protocol was performed; primer concentration at 0.5 μM; dATP, dTTP, dCTP, and dGTP at 0.2 mM; 1× *Pfu* polymerase buffer; 1 mM $MgSO_4$ and 1.25 units of *Pfu*Turbo DNA polymerase were used for the PCR and the amplifications consisted of 30 cycles (1 min at 94 °C, 1 min at 55 °C, and 1.5 min at 72 °C) and a final extension of 10 min at 72 °C. The PCR product was ligated into a pET101 vector.

E. coli strain EB106 (*icd*-11 *dadR*1 *trpA*62 *trpE*61 *tna*-5 *lambda*$^-$) lysogenized by λDE3 [18], was used for expression. Recombinant *Ct*IDH was produced by growing transformed cells in Luria Broth (LB) broth containing ampicillin (100 μg/ml) at 37 °C to $OD_{600\ nm}$ = 0.7–0.8 cell density and subsequent expression (3–4 h) after induction with 1.0 mM isopropyl-β-thiogalactopyranoside (IPTG). After expression, the cells were harvested by centrifugation (5000×*g*, 15 min) and frozen at −20 °C until used. Cells were resuspended in pre-chilled (4 °C) 20 mM sodium phosphate buffer, pH 7.0, containing 10 mM $MgCl_2$ and disrupted using a French pressure cell at 55 megapascals followed by centrifugation (13 000×*g*, 30 min, 15 °C). The purification of *Ct*IDH was performed at room temperature, and the cell extract was loaded directly onto a Red-Sepharose column equilibrated with 20 mM sodium phosphate buffer, pH 7.0 and 10 mM $MgCl_2$. Unbound protein was removed by washing with 0.2 M sodium chloride in 20 mM sodium phosphate buffer, pH 7.0 until A_{280} was zero. An additional washing step was performed using 0.25 mM $NADP^+$ in the sodium phosphate buffer and IDH was then biospecifically eluted by 10 mM DL-isocitrate and 0.25 mM $NADP^+$ in the phosphate buffer. The enzyme was purified to homogeneity (data not shown) as judged by sodium dodecyl sulfate–polyacrylamide gel electrophoresis (SDS–PAGE) with Commassie blue staining, and if the protein was not purified to homogeneity this purification step was repeated. The protein concentration was measured by the method of Bradford [33], using bovine serum albumin as a standard.

2.2. Enzyme assay and determination of the catalytic parameters

IDH activity was measured photometrically (Cary 4E UV–vis spectrophotometer) by monitoring the formation of NADPH at 340 nm (ε_{340} = 6.22 $mM^{-1}\ cm^{-1}$). The standard reaction mixture of 1 ml contained 50 mM Tricine–KOH, pH 8.0, 2 mM DL-isocitrate, 10 mM $MgCl_2$, and 250 μM $NADP^+$. The temperature dependence of catalytic activity and kinetic parameters were studied by assaying the initial IDH activity at different temperatures. The dpK_a/dT of the 50 mM Tricine–KOH buffer was used to ensure that pH 8 was obtained across the temperature range used. For determination of K_m and V_{max} values, the concentration of one substrate was varied while the second was kept at saturating concentration. K_m and V_{max} values were determined from the direct linear plot [34].

Thermodynamic activation parameters were calculated [35], using the following equations:

$$\Delta G^{\#} = RT \times [(\ln K_B T/h) - \ln k] \quad (1)$$

$$\Delta H^{\#} = E_a - RT \quad (2)$$

$$\Delta S^{\#} = (\Delta H^{\#} - \Delta G^{\#})/T \quad (3)$$

where k_B is the Boltzmann constant ($1.3805 \times 10^{-23}\ J\ K^{-1}$), h the Planck constant (6.6256×10^{-34} J s), k (s^{-1}) the rate constant at temperature T (K), E_a the activation energy of the reaction and R ($8.314\ J\ mol^{-1}\ K^{-1}$) the gas constant.

2.3. Thermal stability measurement

Differential scanning calorimetry was carried out with a VP-DSC MicroCalorimeter (MicroCal Inc.) with cell volumes of 0.5274 ml and at a dimer concentration of 22 μM. The calorimetric scans were carried out between 20 °C and 95 °C in 50 mM potassium phosphate buffer, pH 7.5, 0.1 M NaCl, at a scan rate of 1 K/min. A constant pressure of 30 psi was applied to avoid degassing at high temperatures.

2.4. Crystallization, data collection and model building

Two crystal forms of *Ct*IDH were obtained; one in an open conformation (*Ct*IDH-Open) and one quaternary complex with $NADP^+$, isocitrate and Mg^{2+} (*Ct*IDH–NADP). The two *Ct*IDH crystals used for X-ray data collection were both obtained using the hanging drop method, with reservoir solutions of 9–11% (w/v) polyethylene glycol (PEG) PEG3350, and 0.15 M ammonium dihydrogen citrate at 37 °C. Additionally, *Ct*IDH–NADP had 10% (v/v) propylene glycol in the reservoir solution. The drops were made by mixing 3 μl protein with 3 μl reservoir solution. The *Ct*IDH-Open had a protein concentration of 9.5 mg/ml and no additives, whereas the *Ct*IDH–NADP protein solution was at 5 mg/ml also containing 10 mM $NADP^+$ and 10 mM DL-isocitrate. The final crystal sizes were about $1.0 \times 0.2 \times 0.1$ mm^3 for *Ct*IDH-Open and $0.1 \times 0.15 \times 0.3$ mm^3 for *Ct*IDH–NADP. The cryo conditions were 25% glycerol in addition to their respective reservoir solutions and both crystals were flash cooled in liquid nitrogen.

X-ray data were collected at European Synchrotron Radiation Facilities (ESRF), Grenoble at ID29 for the *Ct*IDH-Open crystal, to a final resolution of 2.35 Å The crystal belongs to the space group $P2_1$ with cell parameters $a = 56.15$ Å, $b = 107.25$ Å, $c = 154.59$ Å and $\beta = 93.64°$ and four molecules in the asymmetric unit. The dataset on the *Ct*IDH–NADP crystal was recorded at the macromolecular crystallography beamline BL14.2 at BESSY, Berlin to a final resolution of 2.50 Å (Table 3). The crystal belongs to the space group $P3_221$ with cell axis $a = b = 129.20$ Å and $c = 60.59$ Å. For both the *Ct*IDH data sets the images were integrated and scaled with XDS [36] and structure factors obtained with TRUNCATE [37].

*Ct*IDH–NADP was solved by molecular replacement using 1 monomer of native *Dp*IDH (PDB entry 2UXQ) as search model which has 63/81% sequence identity/similarity. There is one molecule in the asymmetry unit giving a water content of 62%.

It turned out to be more challenging to solve the *Ct*IDH-Open structure in space group $P2_1$, with four monomers in the asymmetric unit giving 52% solvent. Using the program MolRep [37] and one monomer of the open *T. maritima* IDH (*Tm*IDH; PDB 1ZOR) as search model (61/81% sequence identity/similarity) gave four poorly resolved rotation and translation solutions. One model was then built by overlaying each domain from *Dp*IDH (see Fig. 3) onto the open *Tm*IDH structure. This *Dp*IDH-Open-model resulted in four better resolved rotation and translation peaks, where two dimers were found in the asymmetric unit.

The third structure presented here is the complex of *Dp*IDH and $NADP^+$ (*Dp*IDH–NADP) which was obtained by co-crystallization at 8 °C using the hanging drop method and reservoir solutions with 100 mM Tris/HCl buffer at pH 7.4, 1.7–1.9 M ammonium sulfate, 2% PEG 400 and 60 mM magnesium sulfate. The protein solution contained 20 mg/ml *Dp*IDH, 10 mM $NADP^+$ and 10 mM DL-isocitrate, and the drops were made by mixing equal volumes of reservoir (2 μl) and protein (2 μl). The harvested *Dp*IDH–NADP crystal was cryo protected in a solution with 25% glycerol in addition to the reservoir components, and then flash cooled in liquid nitrogen.

Data of *Dp*IDH–NADP were collected at the Swiss-Norwegian Beamlines (SNBL), ESRF, Grenoble, France at 100 K, to 1.93 Å resolution and the complex was found to belong to the space group C2 with cell parameters $a = 61.64$ Å, $b = 98.91$ Å, $c = 71.89$ Å and $\beta = 103.94°$. This is a different crystal form than the native *Dp*IDH (PDB 2UXQ) and *Dp*IDH with only isocitrate (*Dp*IDH-iso; PDB 2UXR) [4]. The X-ray data were integrated and scaled with XDS [36] and the structure factors were obtained using TRUNCATE [37].

The phase problem of *Dp*IDH–NADP was solved by the molecular replacement method using the program MolRep and the native *Dp*IDH (PDB entry 2UXQ) as search model in space group C2. There is one molecule in the asymmetric unit giving a water content of 48%, and the crystallographic twofold axis makes up the functional dimer.

All three models were refined with Refmac5 [38], solvent molecules were added as waters applying the automated ARP_WATERS routine within REFMAC5 and the models were manually inspected in O [39].

2.5. Structural analysis and electrostatic surface calculations

Prior to these calculations all double conformations were removed. Then hydrogen bonds were calculated using the program HBPLUS [40] v3.15 and the following parameters for Donor (D), Acceptor (A), Acceptor Antecedents (AA) and (calculated) Hydrogens (H) were applied: maximum distances for D–A 3.5 Å, H–A 2.5 Å; minimum angle for D–H–A, D–A–AA and H–A–AA of 90°. All ion pairs were included in the calculations. Accessible surface areas were calculated using the program AREAIMOL [37].

Ionic interactions were analyzed using the WHAT IF server (http://swift.cmbi.kun.nl/WIWWWI/), and maximum cut off distances of 4 and 6 Å were applied. Inter-subunit and inter-domain salt bridges were found from the same server with a 4 Å cut-off distance. The qualitative analysis was done in the graphical program O [39]. For each of the three structures dimer were analyzed, for *Ct*IDH-Open from monomer A/B, whereas for *Ct*IDH–NADP and *Dp*IDH–NADP by applying the crystallographic symmetry. Then all hydrogen atoms were added, the electrostatic surfaces were calculated with DelPhi [41] and displayed with PyMol (http://www.pymol.org).

3. Results and discussion

3.1. Biochemical characterization

The optimal growth temperature of the organism *C. thermocellum* ATCC 27405 is 60 °C [42], and it is therefore defined as a thermophile. IDH from this organism (*Ct*IDH) was cloned, the protein expressed and purified for structure determination and biochemical characterization. The thermal stability of *Ct*IDH was determined by differential scanning calorimetry (DSC) under the conditions used previously for *Dp*IDH and *Tm*IDH, which have apparent melting temperatures (T_m) of 66.9 and 98.3 °C, respectively [4,9]. Notably, *Ct*IDH had a T_m of 67.9 °C (Table 1), a temperature only marginally higher than the psychrophilic homolog. The thermophilic *Ct*IDH is active over a broad temperature range spanning a scale from 5 to over 75 °C (Fig. 1) with an apparent optimal enzymatic activity at 70 °C. The fact that the melting temperature is lower than the optimum temperature for activity could be due to experimental differences between the DSC and the activity assay. The DSC thermograms for the thermal denaturation and the determined T_m-values are scan rate dependent (data not shown). The k_{cat} is determined using initial-rate measurements and the enzyme is added to a pre-incubated assay solution, but in the DSC experiments the enzyme is subjected to heat over time.

In order to assess the effect of temperature on the catalytic parameters; enzyme activity k_{cat}, the K_m and the catalytic

Table 1
Thermal properties and kinetic parameters (per catalytic site) for IDHs from subfamily II.

Protein	T_{growth} [a] (°C)	T_{opt} [b] (°C)	T_m [c] (°C)	Assay temp (°C)	NADP			Isocitrate		
					K_m (μM)	k_{cat} (s^{-1})	k_{cat}/K_m (μM^{-1} sec^{-1})	K_m (μM)	k_{cat} (s^{-1})	k_{cat}/K_m (μM^{-1} sec^{-1})
*Ct*IDH	60	70	67.9	5	7.6	3.6	0.5	16.8	3.8	0.2
				25	8.9	35.6	4.0	10	27.4	2.8
				45	11.1	142	12.8	20.6	143	6.9
*Dp*IDH [d]	10	35–40	66.9	5	3.0	7.8	2.6	62.5	4.5	0.07
				25	8.1	35.6	4.4	131	31.4	0.24
				45	41.1	118.6	2.9	4230	115.5	0.03
*Dh*IDH [d]	37	45	58.6	5	13.1	11.7	0.9	23.2	12.2	0.5
				25	29.5	85.8	2.9	20.9	82.0	3.9
				45	108	376	3.5	387	275.8	0.7
*Pc*IDH [e]	39	50	59 [g]	25	5.59	33.3	5.96	8.37	33.3	3.98
*Tm*IDH [d]	80	90	98.3	25	8.6	4.7	0.6	30	4.7	0.2
				45	12.9	34.2	2.7	36.4	35.3	1.0
				70 [f]	55.2 [f]	252 [f]	4.6 [f]	-	-	-

[a] Growth temperature of the organism.
[b] The optimum temperature of the enzyme.
[c] The melting temperature of the enzyme.
[d] Data from Fedøy et al. [4].
[e] Data from Huang and Colman [6].
[f] Data from Steen et al. [15].
[g] Data from Karlstrøm et al. [9].

efficiency k_{cat}/K_m, were determined (Table 1). *Ct*IDH has a similar activity to cold-active *Dp*IDH at 25 °C, but a lower activity than the mesophilic *Dh*IDH. Moreover, at 5 °C *Ct*IDH shows only a slightly lower activity than its psychrophilic and mesophilic homologs (Table 1). K_m-values for isocitrate and $NADP^+$ for *Ct*IDH are lower and less temperature-dependent than the psycro- and mesophilic homologues (Table 1), suggesting a high affinity for both substrate and cofactor in the 5–45 °C temperature range.

An Arrhenius plot ($\ln k_{cat}$ as a function of 1/T) was made of the measurements of k_{cat} at various temperatures and the calculated activation parameters are given in Table 2. The thermodynamic parameters of the experimental data such as the free energy of activation ($\Delta G^{\#}$) for *Ct*IDH is similar to the psychrophilic *Dp*IDH and lower than the hyperthermophilic *Tm*IDH but higher than the mesophilic *Dh*IDH. This may partly explain the overall high activity observed for *Ct*IDH (Fig. 1). The activation energy (E_a) of the reaction increases from psychrophilic to mesophilic and thermophilic and further to hyperthermophilic. This is consistent with earlier observations in other enzyme families [35,43,44]. A low activation energy reduces the thermo-dependence of the reaction rate, an aspect highly important for the psychrophilic enzymes, where it is considered an important adaptation to cold. The activation enthalpy $\Delta H^{\#}$ for *Ct*IDH is higher than the psychrophilic and mesophilic IDHs, giving rise to a thermo-dependent enzymatic activity (k_{cat}) for this thermophilic IDH, displayed by the absolute difference in activity within the temperature range 5–70 °C. In comparison to other IDH enzymes *Ct*IDH has a low activation entropy ($\Delta S^{\#}$) value, both negative and absolute. This is reflected in the low K_m observed for this enzyme, indicating a high affinity for both isocitrate and $NADP^+$. As illustrated in Fig. 1, the *Ct*IDH is a typical thermophilic enzyme with a high activity at its natural working temperature; it is *Dp*IDH that displays an unusual low enzyme activity even at low temperatures. In summary, the thermophilic *Ct*IDH and psychrophilic *Dp*IDH, despite having very different activity rates and temperature optima, nevertheless display similar thermal stability.

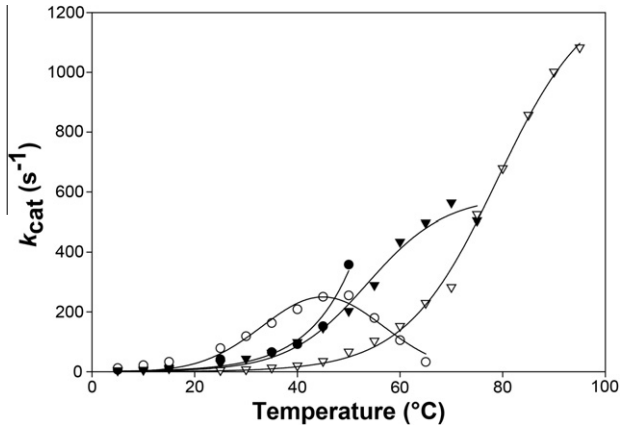

Fig. 1. Specific enzyme activity of the psycrophilic DpIDH (●), the mesophilic DhIDH (○), the thermophilic *Ct*IDH (▼) and hyperthermophilic TmIDH (▽) at saturated conditions.

3.2. The structure determination of CtIDH and DpIDH

In order to link structural differences and properties to the measured differences in biochemical properties between thermophilic *Ct*IDH and psychrophilic *Dp*IDH, crystal structures of thermophilic *Ct*IDH were resolved; one apo form of the enzyme (*Ct*IDH-Open) and one in complex with $NADP^+$, isocitrate and a metal ion (denoted as the *Ct*IDH–NADP). The structure of the cold active *Dp*IDH apo enzyme and in complex with isocitrate was previously determined [4]. Here, we present a quaternary complex crystal structure with $NADP^+$, isocitrate and a metal ion (designated as the *Dp*IDH–NADP). Both complexes were obtained with the same crystallization conditions as the native structures, but crystallized in different space groups.

The open apo form of the structure of *Ct*IDH (*Ct*IDH-Open) was obtained to 2.35 Å resolution and refined to an R-factor and R-free of 21.1% and 26.3% respectively. The space group is $P2_1$ and there are four molecules in the asymmetric unit where monomers A + B and C + D form two dimers. During the refinement two groups of non-crystallographic symmetry (NCS) were applied to the molecule A and C, and B and D, respectively. In addition 16 TLS (Translation/Libration/Screw-motion) groups were used to model anisotropic displacement for the different groups. In the final *Ct*IDH-Open structure many residues are missing including: A1, A134-A139, A305-A321 (17 residues), A402; B1, B306–B324 (19 residues), B402; C1–C2, C134–C139, C210–C214, C306–C321 (16 residues), C402; D1, D306–D324 (19 residues) and D402. In

Table 2
Thermodynamic activation parameters for oxidative decarboxylation of isocitrate to α-ketoglutarate and CO_2 by psychrophilic *Dp*IDH, mesophilic *Dh*IDH, thermophilic *Ct*IDH and hyperthermophilic *Tm*IDH.

	E_a (kJ mol^{-1})	T (°C)	K_{cat} (s^{-1})	$\Delta G^{\#}$ (kJ mol^{-1})	$\Delta H^{\#}$ (kJ mol^{-1})	$T\Delta S^{\#}$ (kJ mol^{-1})	$\Delta S^{\#}$ (kJ K^{-1}mol^{-1})
*Ct*IDH	65.4	5	3.8	66.4	63.1	−3.3	−12.0
		25	27.4	66.5	62.9	−3.6	−12.9
*Dp*IDH [a]	54.8	5	4.5	66.1	52.5	−13.6	−48.8
		25	31.4	66.2	52.3	−13.9	−49.8
*Dh*IDH [a]	58.8	5	12.2	63.8	56.5	−7.2	−26.1
		25	82.1	63.8	56.4	−7.4	−26.7
*Tm*IDH [a]	81.6	25	4.7	70.9	79.1	8.2	29.5
		70	282.7	70.3	78.7	8.4	30.3

[a] Data from Fedøy et al. [4].

Table 3
Statistics from the data collection and refinement statistics for the *Ct*IDH-Open, *Ct*IDH–NADP and *Dp*IDH–NADP structures. The numbers in parentheses represent values in the highest of 10 resolution shells, and the resolution limits for these are indicated.

	*Ct*IDH-Open	*Ct*IDH–NADP	*Dp*IDH–NADP
PDB code	4AOY	4AOU	4AOV
Diffraction data statistics			
Beam line	ID29	BESSY, BL14.2	SNBL
Wavelength (Å)	1.0052	0.9184	0.8536
Resolution limits (Å)	50–2.35 (2.48–2.35)	45–2.50 (2.64–2.50)	40.0–1.93 (2.03–1.93)
Space group	$P2_1$	$P3_221$	C2
Unit cell parameters (Å)	a = 56.2	$a = b$ = 129.2	a = 61.6
	b = 107.3		b = 98.9
	c = 154.6	c = 60.6	c = 71.9
(°)	β = 93.6		β = 103.9
No. unique reflections	75 792	20 411	30 844
Multiplicity	3.4 (3.3)	5.0 (5.0)	3.8 (3.6)
Completeness (%)	99.9 (99.7)	100.0 (100.0)	98.1 (98.1)
$\langle I\rangle/\langle\sigma(I)\rangle$	10.2 (2.1)	13.1 (2.8)	10.7 (2.7)
R_{merge} (%)	8.4 (59.7)	7.1 (61.2)	9.4 (41.4)
Wilson B-factor (Å^2)	46.42	56.17	17.90
Refinement statistics			
Resolution range (Å)	20–2.35	45–2.50	20–1.93
Total reflections	73 524	19 347	29 252
R-factor (%)	21.13	18.93	17.49
R-free (%)	26.32	24.40	22.54
No./size (%) of R-free set	2010 (2.7)	1 043 (5.1)	1563 (5.1)
No. of protein atoms	11 934	3 210	3 249
No. of water molecules	88	41	227
No. of other molecules	–	1 Mg^{2+}, 1 isocitrate, 1 $NADP^+$	1 Mg^{2+}, 1 isocitrate, 1 $NADP^+$
Average B factor (Å^2)			
Total	27.0	45.2	20.1
Protein A/B/C/D	27.1/26.8/26.9/27.0	45.2	19.9
Water/Mg^{2+}/iso./$NADP^+$	34.7/–/–/–	42.9/43.0/37.9/52.1	25.0/6.0/12.9/13.3
RMSD from ideal geometry			
Bonds (Å)	0.015	0.017	0.012
Angles (°)	1.67	1.88	1.41
Ramanchandran plot			
Core (%)	89.3	89.0	93.3
Allowed (%)	9.8	9.6	6.1
Generously allowed (%)	0.5 (6 residues)	1.1	0.3
Disallowed (%)	0.5 (6 residues)	0.3 (1 residue)	0.3 (1 residue)

particular, it is striking that the helix α11 is missing in all four monomers, where 16–19 residues in each helix are not defined in the crystal structure (Fig. 2). There are 88 water molecules and the overall and avarage B-factors for each monomer are lower than the Wilson B-factor (Table 3).

A 2.5 Å crystal structure of *Ct*IDH with $NADP^+$ (*Ct*IDH–NADP), a metal interpreted as magnesium, isocitrate and the majority of the $NADP^+$ were clearly defined in the 2Fo-Fc electron density, except for the nicotinamide moiety of $NADP^+$ which was not defined (Fig. 3a and c). The final model refined to an R-factor of 18.9% and an R-free of 24.4%. There are 41 water molecules, some side-chains were refined with zero occupancy and the mean B-value of the protein is 45.2 Å^2, which is in the same order as the Wilson B-factor (Table 3).

The final model of *Dp*IDH–NADP was refined to 1.93 Å resolution and to an R-factor and R-free of 17.5% and 22.5%, respectively. There is one molecule in the asymmetric unit and the functional dimer is generated by the crystallographic twofold axis. The observed electron density maps clearly define one magnesium ion, one isocitrate with reasonable B-values (Table 3) and the majority of the $NADP^+$ co-factor is defined (Fig. 3b and d). The exception is the nicotinamide group adjacent to the isocitrate for which no electron density was seen. The resulting phosphor-ADP-ribose could then be derived from an $NADP^+$ molecule by hydrolysis of

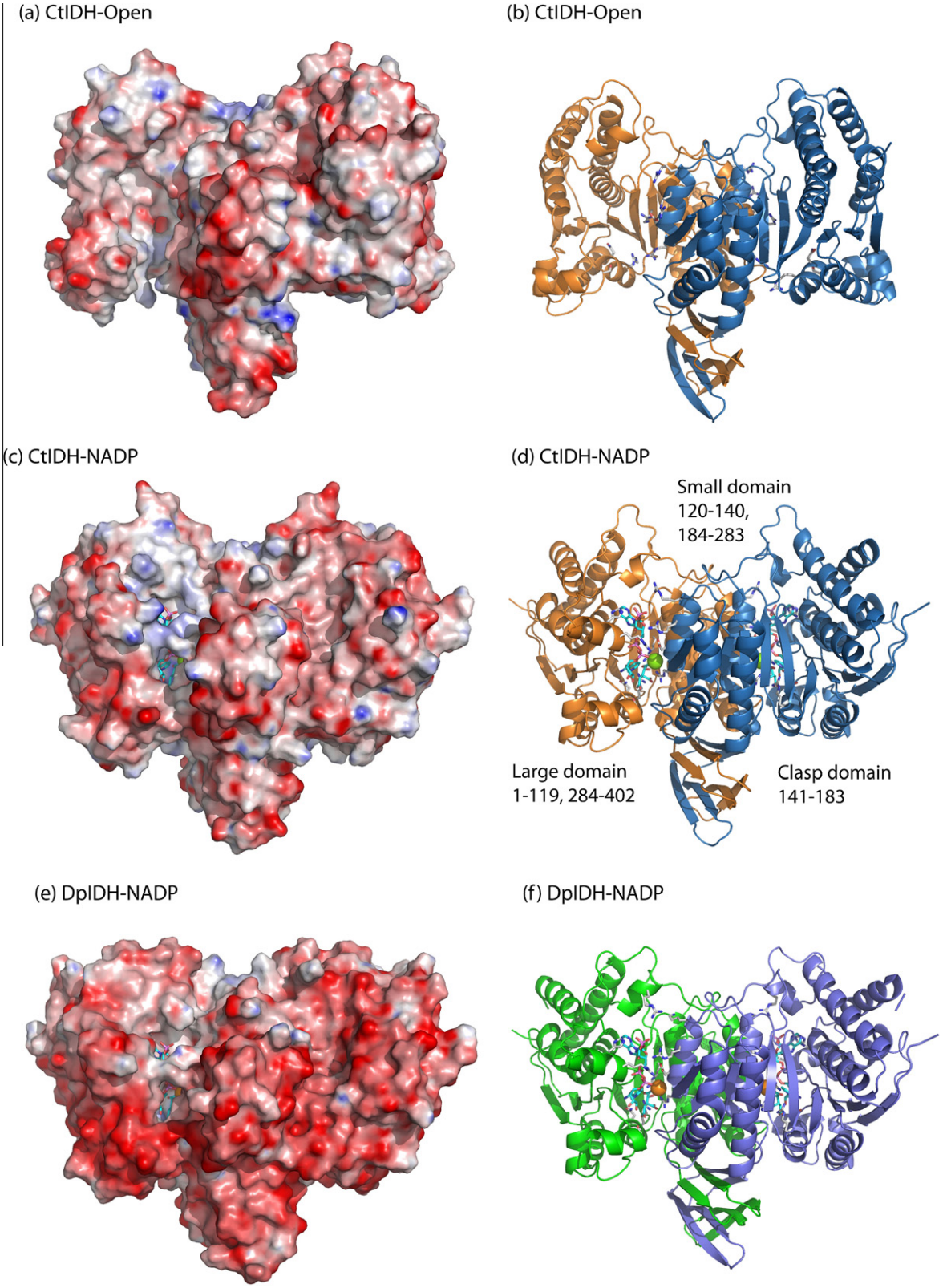

Fig. 2. Calculated electrostatic surface potentials (left panels) and ribbon diagrams (right panels) of *Ct*IDH-Open (a and b) *Ct*IDH–NADP (c and d) and *Dp*IDH–NADP (e and f). The colors red, white and blue indicate charge potentials of −10, 0 and +10 K_bT/e, respectively.

the nicotinamide group as also observed for an NADPH dependent alcohol dehydrogenase [45]. See Table 3 for further details from the three refined structures.

The sequence alignment of the IDHs displays the conservation of secondary structural elements and active site amino acid residues (Fig. 4). *Ct*IDH-Open is more similar to *Tm*IDH with lower

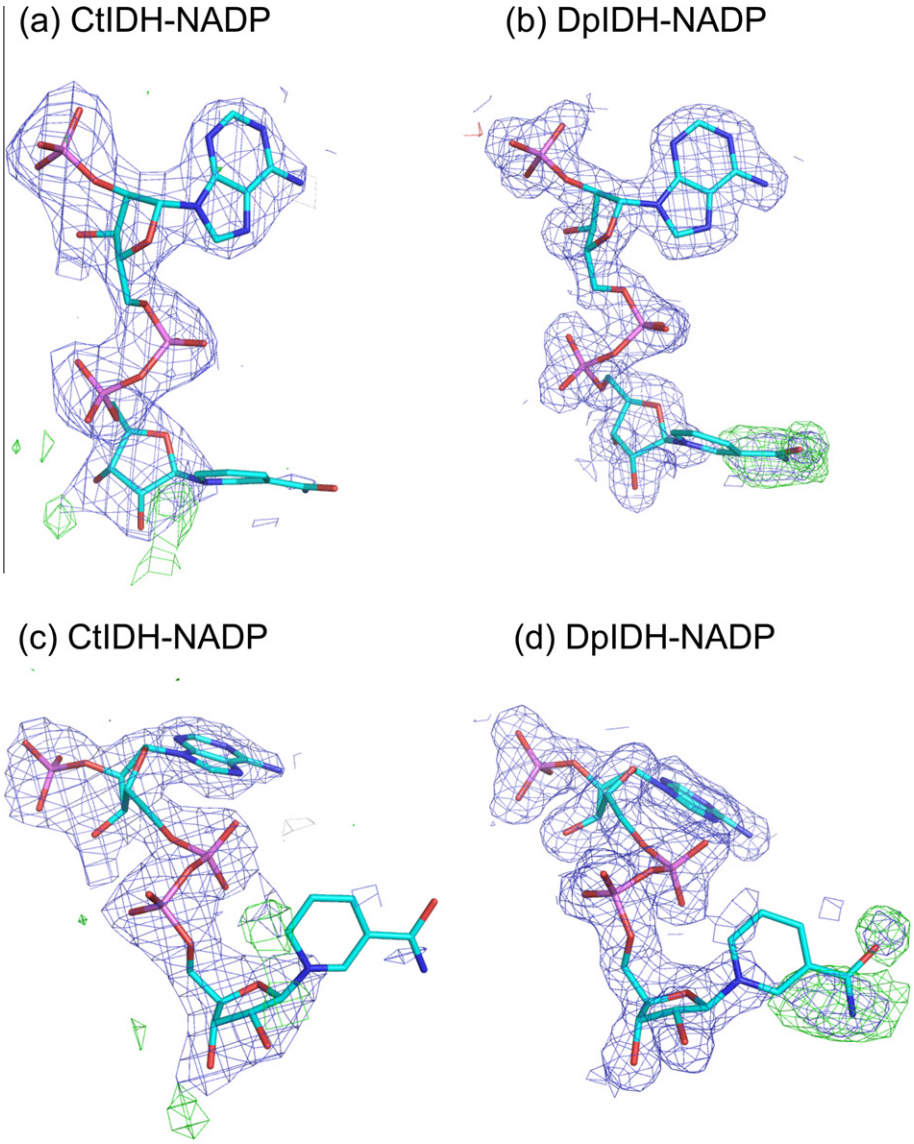

Fig. 3. Observed 2Fo-Fc electron density (1σ; blue) and difference Fo–Fc electron density (3.5σ; green) for the NADP molecules in the final models of *Ct*IDH–NADP (panels a and c) and *Dp*IDH–NADP (panels b and d). The molecules were refined with occupancy 0 for 8 of the atoms in the nicotinamide group. A similar phosphate ADP-ribose molecules was also observed for the NADP molecule bound to alcohol dehydrogenase from *Saccharomyces cerevisiae* [45].

RMSD score and most of the secondary structure elements in all three domains have comparable conformations. When superimposing one monomer of *Ct*IDH-Open onto *Ct*IDH–NADP using the CA-atoms in the small domains and the clasp domains only, the movements include most residues in the large domain, specifically residues 2–106 and 290–402 have different conformations. Ser2 in *Ct*IDH-Open has moved 16.9 Å relative to Ser2 in the closed conformation of *Ct*IDH–NADP (Fig. 5a and b). In one IDH monomer there is a long beta sheet with 10 β-strands for which five strands can overlap in the two *Ct*IDH structures and then the next five β-strands have different orientations in *Ct*IDH-Open and *Ct*IDH–NADP as partly illustrated in Fig. 5. The CA atom of Asn38 is displaced by 13 Å in *Ct*IDH-Open relative to *Ct*IDH–NADP, and the large domain of *Ct*IDH-Open is rotated about 30° compared to the closed *Ct*IDH–NADP as measured by the angle between Asn38 (open)-Arg109-Asn38 (closed) within one monomer. In the open structures of *Tm*IDH and human cytosolic IDH (*Hc*IDH; PDB 1T09) the same angle was found to be ∼30° and ∼24° respectively [9,16], thus in this sense *Ct*IDH-Open is most similar to *Tm*IDH.

The new *Dp*IDH–NADP structure presented here is most similar to *Dp*IDH-iso (with isocitrate) for which only residues 308–318 in helix α11 are positioned closer to the small domain in the *Dp*IDH–NADP structure. The two presented quaternary complex structures (*Ct*IDH–NADP and *Dp*IDH–NADP) are also similar with low RMSD, helix α11 at comparable positions and only some differences for residues at the termini of secondary structure elements.

3.3. Structural contributions to stability and flexibility

Structural analyses of hydrogen bonds, ion-pairs and inter-subunit interactions are summarized in Table 4, in order to relate structure to observed apparent melting points. Overall the number of hydrogen bonds is high at 0.995 per residue for both *Ct*IDH–NADP and *Dp*IDH–NADP though *Ct*IDH has more main-chain to main-chain hydrogen bonds. There are more ion-pairs in *Ct*IDH–NADP (28) than in *Dp*IDH (both with NADP (25) and native (24)) and many of these are located in clusters involving three amino acids (Table 4). There are fewer inter-subunit hydrogen bonds and fewer inter-subunit ion-pairs in *Ct*IDH–NADP than

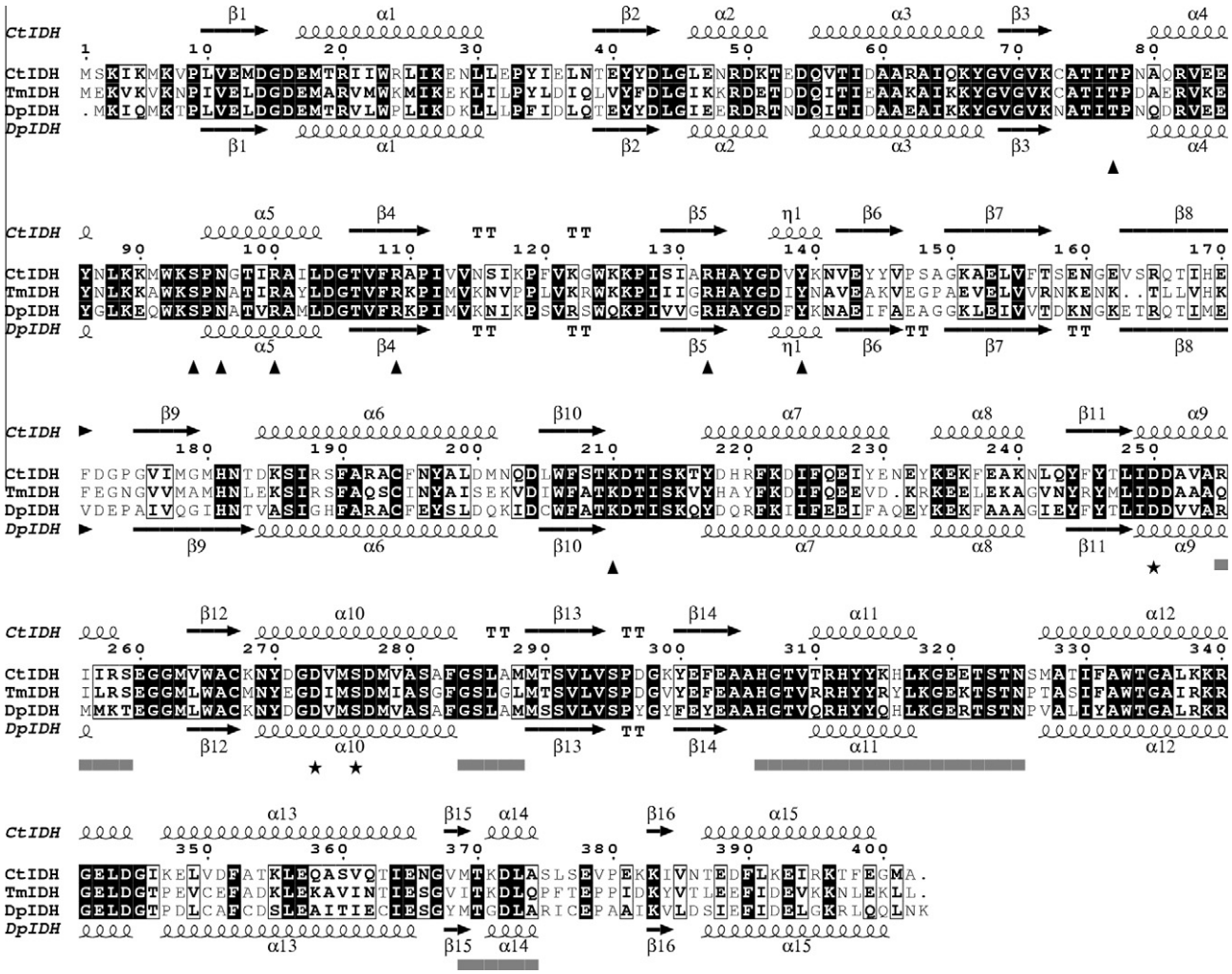

Fig. 4. Sequence alignment of isocitrate dehydrogenase from *Clostridium thermocellum* (*Ct*IDH), *Thermotoga maritima* (*Tm*IDH) and *Desulfotalea psychrophila* (*Dp*IDH). The secondary structure elements of *Ct*IDH–NADP (top) and *Dp*IDH–NADP (bottom), the isocitrate binding residues (★), the metal binding residues (▲) and NADP binding regions (■) are indicated.

in *Dp*IDH–NADP and *Dp*IDH, and only two such inter-subunit ionic interactions were found in *Ct*IDH–NADP. The different domains in *Ct*IDH–NADP are connected with a comparable number of interactions as in *Dp*IDH, but there are more hydrogen bonds from the clasp to the small domain in *Ct*IDH–NADP. The dimer interface has comparable sizes in *Ct*IDH–NADP and *Dp*IDH–NADP (Table 4). For the *Ct*IDH-Open structure the numbers of interactions are generally fewer, probably due to the resolution and possibly also the open conformation. By comparing *Ct*IDH-Open to the *Tm*IDH open structure (T_m = 98.3 °C), there are no 5-member ion-pair clusters (<4.0 Å) and a much lower number of hydrogen bonds per residue was found in *Ct*IDH-Open (0.855) compared to *Tm*IDH (0.980) [4]. The very high thermal stability of *Tm*IDH is primarily explained by the abundance of large strategically placed ion pair clusters, and their absence in *Ct*IDH probably explains its moderate T_m. What is striking is the high number of polar residues in *Ct*IDH (30.6%) compared to *Dp*IDH (22.9%), and many polar residues are also found in *Pc*IDH, *Hc*IDH and *Tm*IDH (see Table 3 in Fedøy et. al., 2007) [4]. So totally, one *Ct*IDH–NADP monomer is stabilized with many hydrogen bonds and more three member ion-pair networks than in *Dp*IDH, while there are fewer inter-subunit interactions. This might account for the comparable T_m values found for *Ct*IDH and *Dp*IDH.

The net charges of the *Ct*IDH and *Dp*IDH dimers are −12 and −24, respectively, with charged N and C termini and neutral histidines. The calculated electrostatic surface potentials of the three crystal structures are shown in Fig. 2, it is clear that both *Ct*IDH structures are less negatively charged than *Dp*IDH, even if the *Ct*IDH-Open structure is slightly more negatively charged due to disordered missing residues. In particular, the $NADP^+$ binding cleft in *Ct*IDH is more neutral than the negatively charged one found in *Dp*IDH (Fig. 2).

In *Dp*IDH an enlarged aromatic cluster was found in each of the small domains [4] and mutation of Phe205Met in *Tm*IDH (Phe207 in *Ct*IDH) resulted in a decrease in T_m by −3.5° C [9]. This aromatic cluster in *Ct*IDH has the same size as in *Dp*IDH with 11 aromatic residues (residues 190, 195, 207, 217, 221, 225, 229, 233, 237, 244, 246) which is bigger compared to *Tm*IDH with 7 aromatic residues.

In the clasp domain of the *Ct*IDH–NADP structure there are some ion-pair interactions which include Glu170-Lys151, Lys151-Glu153, Glu153-Arg165 where only the latter is <4 Å and is therefore considered to be the strongest. Compared to *Dp*IDH–NADP the clasp domain in *Ct*IDH–NADP is less stabilized by ionic interactions, but slightly better bounded to the small domain by hydrogen bonds (Table 4).

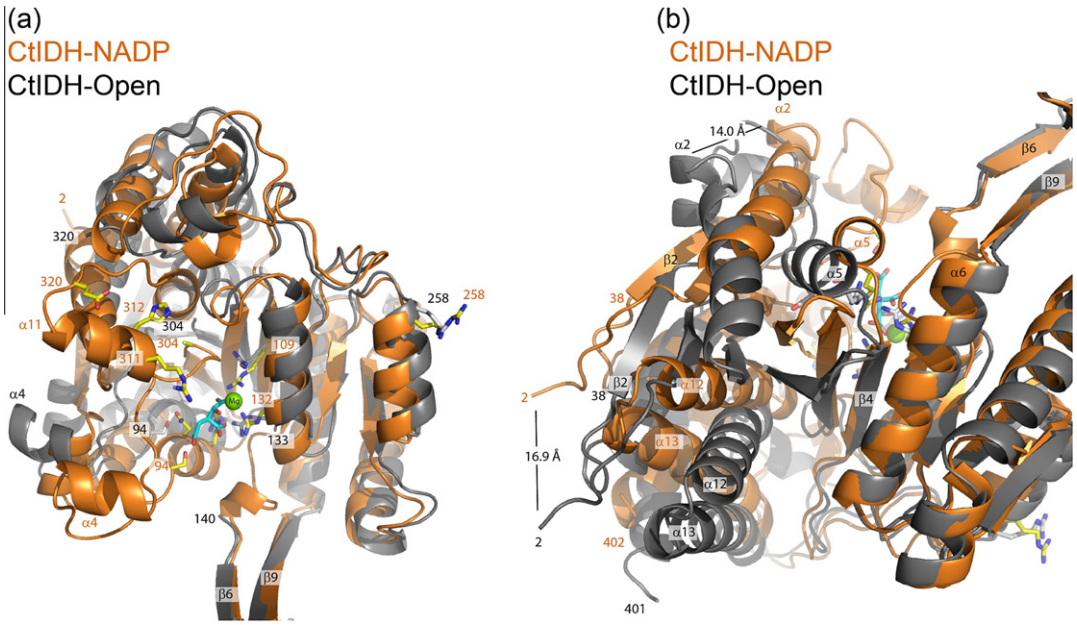

Fig. 5. Comparison of monomer A of *Ct*IDH–NADP (orange) and *Ct*IDH-Open (gray) after super-positioning on the small domain (120–140, 184–283) and the clasp domain (141–183). Panels (a) and (b) have different orientations, some residues and secondary structure elements are outlined, and the distance between the CA-atoms of Ser2 and Thr52 in *Ct*IDH–NADP and *Ct*IDH-Open are indicated.

Table 4
Structural analysis and characteristics of *Ct*IDH-Open, *Ct*IDH–NADP, *Dp*IDH–NADP and *Dp*IDH.

	*Ct*IDH-Open	*Ct*IDH–NADP	*Dp*IDH–NADP	*Dp*IDH (PDB 2UXQ)[$]
Apparent melting temperature (°C)	67.9		66.9[$]	
No of amino acids in monomer A in PDB (in gene)	378 (402)	401 (402)	402 (402)	402 (402)
Hydrophobic residues[a] (%)	39.8		48.6	
Polar residues[b] (%)	30.6		22.9	
Charged residues[c] (%)	29.6		28.5	
Resolution (Å)	2.35	2.50	1.93	1.75
No of hydrogen bonds per residue in monomer A	0.855	0.995	0.995	0.739
No of SS[d] hydrogen bonds per residue	0.108	0.150	0.167	0.070
No. of SM[e] hydrogen bonds per residue	0.159	0.137	0.179	0.107
No. of MM[f] hydrogen bonds per residue	0.640	0.708	0.647	0.562
No. of ion pairs per monomer at 4/6 Å	17/50	28/61	25/54	24/54
No. of ion pairs per residue (4 Å)	0.045	0.070	0.062	0.060
No. of 2 member networks in monomer A at 4.0 Å	12	14	15	18
No. of 3 member networks in monomer A at 4.0 Å	4	6	5	3
No. of inter-subunit hydrogen bonds	28	44	51	33
No. of inter-subunit ion pairs at 4.0 Å	1	2	6	4
No. of inter-subunit 2 member network at 4.0 Å	1	0	2	3
No. of inter-subunit 3 member network at 4.0 Å	0	2	4	0
No. ion pairs < 6.0 Å (<4.0 Å)/No. hydrogen bonds between:				
Large–small domain	3 (1)/11	4 (0)/12	5 (0)/14	3 (1)/11
Large′–small domain	1 (1)/11	4 (0) / 12	5 (0)/14	4 (1)/16
Clasp–small domain	0 (0)/14	0 (0)/28	0 (0)/22	0 (0)/25
Accessible surface area of dimer (Å^2)	31480	30118	30044	29343
Buried inter-subunit surface (% of dimer)	30.2	30.1	30.1	30.1

[$] Data from Fedøy et al. [4].
[a] Hydrophobic residues: A,V,L,I,W,F,P,M.
[b] Polar residues: G,S,T,Y,N,Q,C.
[c] Charged residues: R,K,H,D,E.
[d] SS, side-chain–side-chain hydrogen bonds.
[e] SM, side-chain–main-chain hydrogen bonds.
[f] MM, main-chain–main-chain hydrogen bonds.

Stabilization of the N and C termini has been found to be important for thermal stability in hyperthermophilic IDHs [8,9,18]. The first prominent difference between *Ct*IDH and the other IDH homologs was the disruption of a conserved ion-pair due to a mutation of a lysine to aspargine. In *Tm*IDH one ion-pair Lys29-Asp389 was found to stabilize the structure substantially, since if it was disrupted the T_m decreased by -21.8 °C. This ionic interaction is also present in *Dp*IDH, *Pc*IDH and *Hc*IDH [4,9], but the corresponding interaction is not found in *Ct*IDH due to mutations corresponding to Asn29 and Glu393. Still, in the same region of *Ct*IDH–NADP there

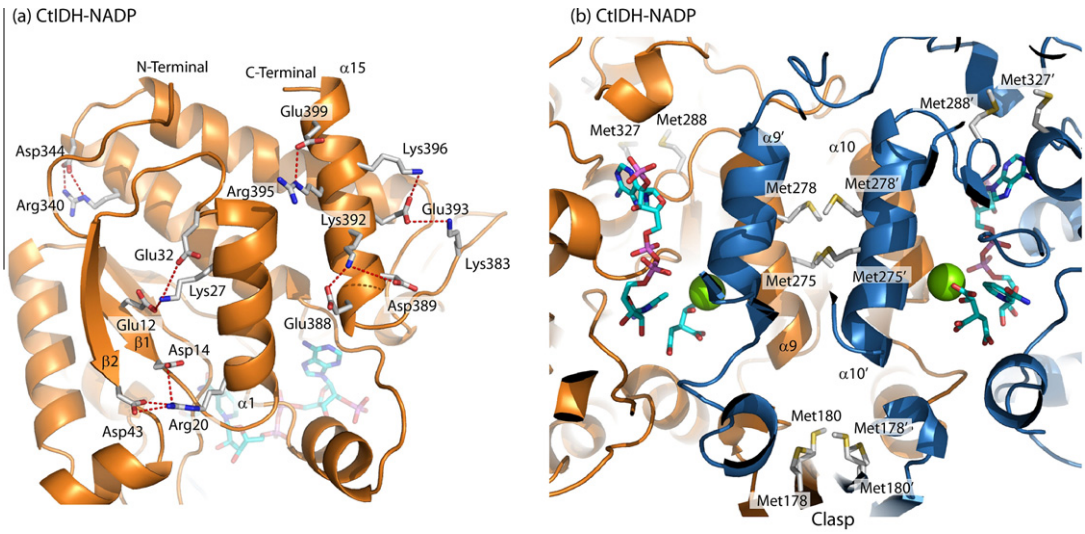

Fig. 6. (a) Ionic interactions in the N and C termini of *Ct*IDH–NADP. (b) Two four member Met-clusters at the dimer interface of *Ct*IDH–NADP and two adjacent Met residues (327, 288). More details are described in the text.

are three locally stabilizing interactions involving Lys383-Glu393-Lys396, Glu388-Lys392-Asp389 and Arg395-Glu399 and a hydrogen bond from Glu399 to Tyr34 (Fig. 6a). In addition there are ionic interactions connecting Glu12-Lys27-Glu32 (Fig. 6a). Finally, two short strong ionic interactions involving Arg340-Asp344 are found in *Ct*IDH–NADP and also extended by two hydrogen bonds (Asp344-Val8, Arg340-Tyr67) in the same region (Fig. 6a). The N and C termini of *Ct*IDH–NADP seem to be stabilized by other ionic interactions than in *Dp*IDH and *Tm*IDH, but still the number of ionic interactions is high and several hydrogen bonds are well defined, which probably all together stabilize the *Ct*IDH structure.

The number of methionine residues in *Ct*IDH, *Dp*IDH and *Tm*IDH are 16 (4.0%), 14 (3.5%) and 13 (3.3%) respectively, and their locations in the structure have been analyzed. In *Dp*IDH a large methionine cluster has been described at the dimer interface with six adjacent Met-residues [4]. At the dimer interface of *Ct*IDH the cluster is smaller with Met275, Met278, Met275′ and Met278′ adjacently positioned, and interestingly *Ct*IDH also has another cluster in the clasp domain with Met178, Met180, Met178′ and Met180′ (Fig. 6b). Both these clusters are also found in *Tm*IDH. For the remaining Met-residues most of them are distributed throughout in the structures, but unique to *Ct*IDH are Met327 and Met288 in the large domain which are facing each other. The role of the Met-clusters in *Ct*IDH could be to maintain the flexibility of the enzyme during catalysis and thus affect the catalytic rate.

The detailed structural investigations of *Ct*IDH display typical thermophilic structural characteristics with a higher number of hydrogen and ionic interactions per residue than the mesophilic homologs *Pc*IDH and *Hc*IDH [1,16]. Moreover, fewer ionic interactions and only three-member ion-pair networks and not the enlarged ionic networks were found in *Ct*IDH as compared to the hyperthermophilic *Tm*IDH and *Ap*IDH [8,9].

3.4. Active site

The amino acids involved in the binding of cofactor and substrate are highly conserved in all IDH enzymes. In the active site of *Ct*IDH–NADP the isocitrate ion is bound to the conserved positively charged residues Arg100, Arg132, Arg109, and Lys210′, and hydrogen bonds are made to Ser94, Asn96, Thr77, Tyr139, Asp250′ and Asp273 (Fig. 7b). The orientation of the isocitrate and the interacting residues in *Ct*IDH–NADP are very similar to *Dp*IDH-iso (PDB 2UXR) and *Dp*IDH–NADP (Fig. 7e). The metal is interpreted as Mg^{2+} and is penta-coordinated by a water molecule (W2), Asp250′, Asp273 and by two oxygen atoms in the isocitrate in a bidentate mode. Additionally W2 is stabilized by binding to Asp277.

In *Dp*IDH–NADP the isocitrate interactions residues are found at almost identical positions as in *Dp*IDH-iso, but one difference is the octahedral-geometry of the magnesium by an additional water molecule (not labeled but shown in Fig. 7e). Further details on differences in bonds lengths and the number of hydrogen bonded water molecules have not been examined due to the different resolutions (2.5 Å versus 1.93 Å) of the compared structures.

In both complex structures presented, *Ct*IDH–NADP and *Dp*IDH–NADP, one metal, one isocitrate and one apo-NADP (lacking the nicotinamide group) are found in the active sites. For *Ct*IDH–NADP the mean B-value of the cofactor is 52.1 $Å^2$ which is quite high. Still the observed electron density map clearly indicated the presence of the cofactor except for 8 atoms in the nicotinamide group which was refined with zero occupancy. For the rest of the cofactor, the three phosphate groups and the adenine moiety are nicely defined in the electron density (Fig. 3a and c). Due to the lack of electron density of the C_4 of the nicotinamide moiety, which has been shown to be the involved in the initial hydride transfer, we could not perform a more thorough investigation of the acid–base chemistry.

Both quaternary complexes reveal that the 2′-phosphomonoester group forms ion pairs to His312 (*Ct*IDH) and Arg255′ (*Ct*IDH)(Fig. 7a and c). The tight interaction found for His312 to $NADP^+$ in the presented crystal structure (Fig. 7c), further supports the importance of this residue in the binding of $NADP^+$. Similar interactions are observed within all known structures of subfamily II IDH [16,32], also mutational studies in *Pc*IDH confirm the importance of this histidine [46]. The ionic interactions between the Arg255′ (*Ct*IDH) or Arg254′ (*Dp*IDH) to the 2′-phosphomonoester group of $NADP^+$ are unique for *Ct*IDH and *Dp*IDH, therefore this arginine residue may represent a different cofactor discriminating interaction. In the other known structures there is a Glutamine (Gln) in this position [9,16,32], making a hydrogen bond to the 2′-phosphomonoester in *Sc*IDH (Gln259′). The conformation of Arg255′ is stabilized by the ion pair formation to Asp251′. In addition, a more basic/neutral environment in the binding pocket in the vicinity of the 2′-phosphomonoester, seems more complementary to the negatively charged phosphate-group in *Ct*IDH compared to *Dp*IDH (Fig. 2c and e).

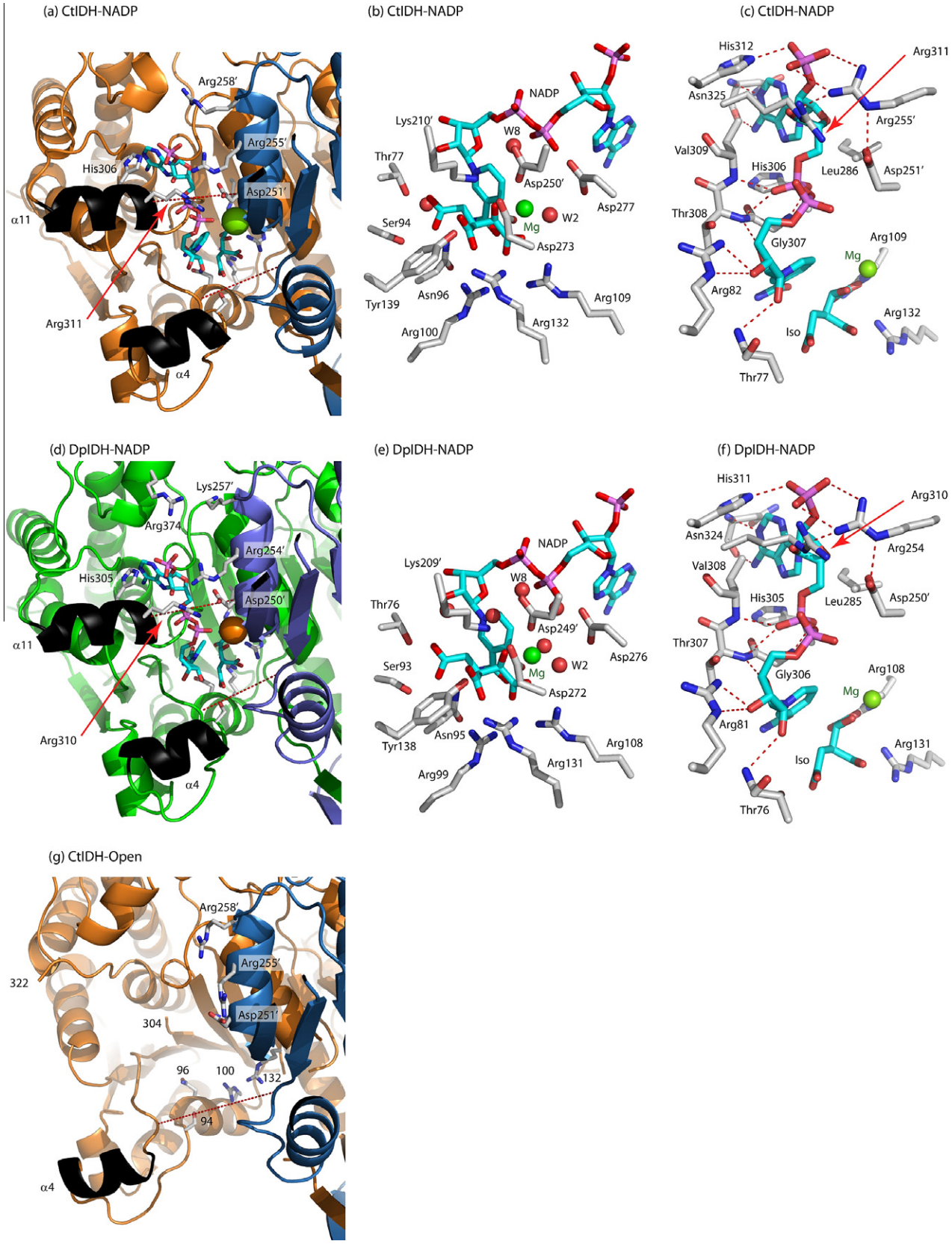

Fig. 7. The NADP and isocitrate binding clefts (left panels) in (a) *Ct*IDH-NAPD, (d) *Dp*IDH–NADP and (g) *Ct*IDH-Open. Isocitrate binding residues (middle panels) in the (b) *Ct*IDH–NADP and (e) *Dp*IDH–NADP crystal structures. The $NADP^+$ interacting residues in (c) *Ct*IDH–NADP and (f) *Dp*IDH–NADP not including the hydrogen bonded water molecules. For $NADP^+$ the non-defined NADP nicotinamide groups are also including.

In *Dp*IDH–NADP the cofactor to protein interactions are similar as described in *Ct*IDH–NADP, with His311 and Arg254′ forming ionic interactions to the 2′-phosphomonoester group. In addition, Arg374 is pointing towards the 2′-phosphomonoester group and

Table 5
Defined widths of the $NADP^+$ and isocitrate binding sites as also shown in Figure 7.

	*Ct*IDH-Open	*Tm*IDH (Open)	*Dp*IDH	*Dp*IDH-Iso	*Ct*IDH–NADP	*Dp*IDH–NADP
PDB entry	4AOY	1ZOR	2UXQ	2UXR	4AOU	4AOV
Width of NADP site (Å)[a]		18.7	15.6	13.0	11.8	11.8
Width of isocitrate (Å) site[b]	19.6	18.5	11.7	10.6	10.5	10.4
RMSD for CtIDH-Open (Å)[c] (no of CA atoms)		1.22 (364)	2.65 (363)	2.94 (345)	2.80 (334)	3.17 (350)
RMSD for CtIDH-NADH (Å)[c] (no of CA atoms)		2.44 (348)	1.31 (400)	0.93 (398)		0.85 (392)

[a] Distance corresponding to Arg311 CA – Asp251′ CA in CtIDH, Arg310 CA – Asp250′ CA in DpIDH,
[b] Distance corresponding to Thr77 CA – Lys210′ CA in CtIDH, Thr76 CA – Lys209′ CA in DpIDH.
[c] RMSD for the most similar monomers.

is 4.5 Å away from one of the oxygen atoms in the cofactor (Fig. 7d), thus forming a weak ionic interaction. For *Dp*IDH–NADP the adenine moiety has both hydrophobic and hydrophilic interactions with the side-chains of Leu285, Val308, His305, Asn324 and His311. In particular there are two short hydrogen bonds from the main chain of Asn324 N and O to the N1 and N6 atoms of the adenine, respectively (Fig. 7f). In *Ct*IDH Asn325 makes the same interactions. The nature and total number of interactions may explain the high affinity found for $NADP^+$ for both *Dp*IDH and *Ct*IDH.

However, by comparing the $NADP^+$ interactions in *Ct*IDH–NADP and *Dp*IDH–NADP to those found in *Hc*IDH (PDB 1T0L) and *Sc*IDH (PDB 2QFX) one of the largest differences is the interactions of the 3′OH group of the adenosine ribose moiety. In *Ct*IDH–NADP there is a short interaction (3.3 Å) from Arg255′ to the 3′OH group of the adenosine ribose moiety and a similar interaction is found in *Dp*IDH–NADP (3.4 Å; Fig. 7c and f). Whereas in the quaternary *Sc*IDH complex [32], it is the Arg316 in the large domain (Arg311 in *Ct*IDH) that is stabilizing the same 3′OH group with a distance of only 2.8 Å. In the Arg311 equivalent in *Hc*IDH (Arg314) this distance is only 3.2 Å. Hence, the interactions to the 3′OH group of the adenosine ribose are from the small domain in the *Ct*IDH and *Dp*IDH, whereas for *Sc*IDH and *Hc*IDH the interactions are from the large domain.

The number of water molecules hydrogen bonded to the $NADP^+$ molecules in the two presented structure are different, probably reflected by the difference in resolution (2.50 Å for *Ct*IDH–NADP and 1.93 Å for *Dp*IDH–NADP), and these interactions are therefore not investigated in more detail.

3.5. Opening and closure of the overall structures: a unique active site locking mechanism

A profound difference between subfamily I and subfamily II IDHs is the insertion of two extra α-helices, α4 and α11, in the subfamily II enzymes. For the eukaryotic *Sc*IDH [32] these helices were proposed to be important for a more fine-tuned and complex catalytic mechanism compared to *Ec*IDH. The accepted catalytic mechanism for *Ec*IDH which is from subfamily I, is a random binding of substrate and cofactor leading to the ordered enzyme-substrate complex [2,7,20–24]. In *Sc*IDH these α-helices act as a lid by covering the top of the $NADP^+$- and isocitrate-binding site and as a result the entrance of the active site is significantly narrowed. In the comparison of the closed *Ct*IDH–NADP and the *Ct*IDH-Open structure (Fig. 5) the movement of the α4 helix is evident. The fact that the electron density is not defined for α11 in any of the four molecules in *Ct*IDH–NADP, indicates high flexibility in this structural element and leads to the perception that the α11 helix is moving and is adaptable upon opening of the $NADP^+$ binding site. From our earlier work we observed that helix α11 and Arg310 also moved comparing the native *Dp*IDH to the *Dp*IDH-Iso (PDB 2UXR) structure [4]. In the *Dp*IDH-Iso structure Arg310 is defined in the electron density map and α11 moved closer to the small domain forming a narrower $NADP^+$ binding site. In the new *Dp*IDH–NADP structure presented here, the width of the $NADP^+$ site is even shorter (Table 5) and the helix α11 (see Fig. 7d) closes the $NADP^+$ site more tightly than in *Dp*IDH-Iso. We do not suspect the crystal packings are responsible for the observed movements and changes. The conformation of α11 and Arg311 (Arg310 in *Dp*IDH) in *Ct*IDH–NADP is very similar to *Dp*IDH–NADP (Fig. 7a and d). Therefore we suggest a new model of the active site locking mechanism (Fig. 8); where we present one open-*Ct*IDH and one locked *Ct*IDH–NADP structure, an open *Tm*IDH structure, a closing structure of the apo native *Dp*IDH and a closed complex structure with isocitrate of *Dp*IDH-Iso reported earlier [4], and a locked structure of *Dp*IDH–NADP; which together provides a detailed overview of the important domain movements for efficient catalysis.

In our new model (Fig. 8) the most open structure is *Ct*IDH-Open with a isocitrate binding site width of 19.6 Å (Table 5) and the α11 not defined in the electron density. Then in *Tm*IDH, α11 is defined and the $NADP^+$ and isocitrate sites are still wide (18.7 Å and 18.5 Å) but smaller than the former. The apo native *Dp*IDH is defined as a closing state, because even if the complete large domain is clearly shifted towards the small domain (compared to the open state), the main-chain is still around 2 Å more open than the closed *Dp*IDH-Iso structure with bound isocitrate. Finally the most locked states are represented by the structures of the quaternary complexes with $NADP^+$, isocitrate and Mg^{2+}, (*Ct*IDH-NAPD, *Dp*IDH-NAPD) as reflected by the most narrow $NADP^+$ and isocitrate sites. These quaternary structures could represent a productive conformation of the protein, with substrate and cofactor ready for catalysis. All the domain movements are also reflected by the RMSD towards *Ct*IDH-Open or *Ct*IDH-NAPD (Table 5).

The importance of the α4 and α11 helices is also seen in our structures. Firstly, α11 is disordered (*Ct*IDH-Open) and then it becomes ordered and moves closer to the active site, as displayed by the closing state of the apo native *Dp*IDH (2UXQ), but the Arg311 equivalent (Arg310) makes no interactions and is not defined. Further movement of α11 closes the active site, as displayed in *Dp*IDH-iso, and then finally locking of α11 onto the active site cleft by the unique interactions from Arg311 to Asp250′ and also Arg255′ (*Ct*IDH–NADP, *Dp*IDH–NADP). Asp250′ enables and helps Arg255′ to interact with the $NADP^+$ cofactor and stabilize the 3′OH group of the adenosine ribose moiety (Fig. 7c and f). Secondly, α4 is first positioned far away (19.6 Å in *Ct*IDH-Open; Table 5), and becomes closer when α11 is defined (11.7 Å, apo native *Dp*IDH) and even tighter when isocitrate and/or $NADP^+$ is bound (10.4–10.6 Å; *Ct*IDH–NADP, *Dp*IDH–NADP, *Dp*IDH-Iso). The closing of large domain and the movement of α11 and the locking by Arg311 to the small domain, together with residue determinants from both the large (His312) and the small domain (Arg255′) for the $NADP^+$ selectivity are important subtle movements in *Ct*IDH and *Dp*IDH, regulating their catalytic efficiency and selectivity.

The crystal structures of the thermophilic IDH from *C. thermocellum* fill the gap in the temperature scale within subfamiliy II. The bacterial homologs in this study (*Dp*IDH, *Dh*IDH, *Ct*IDH and

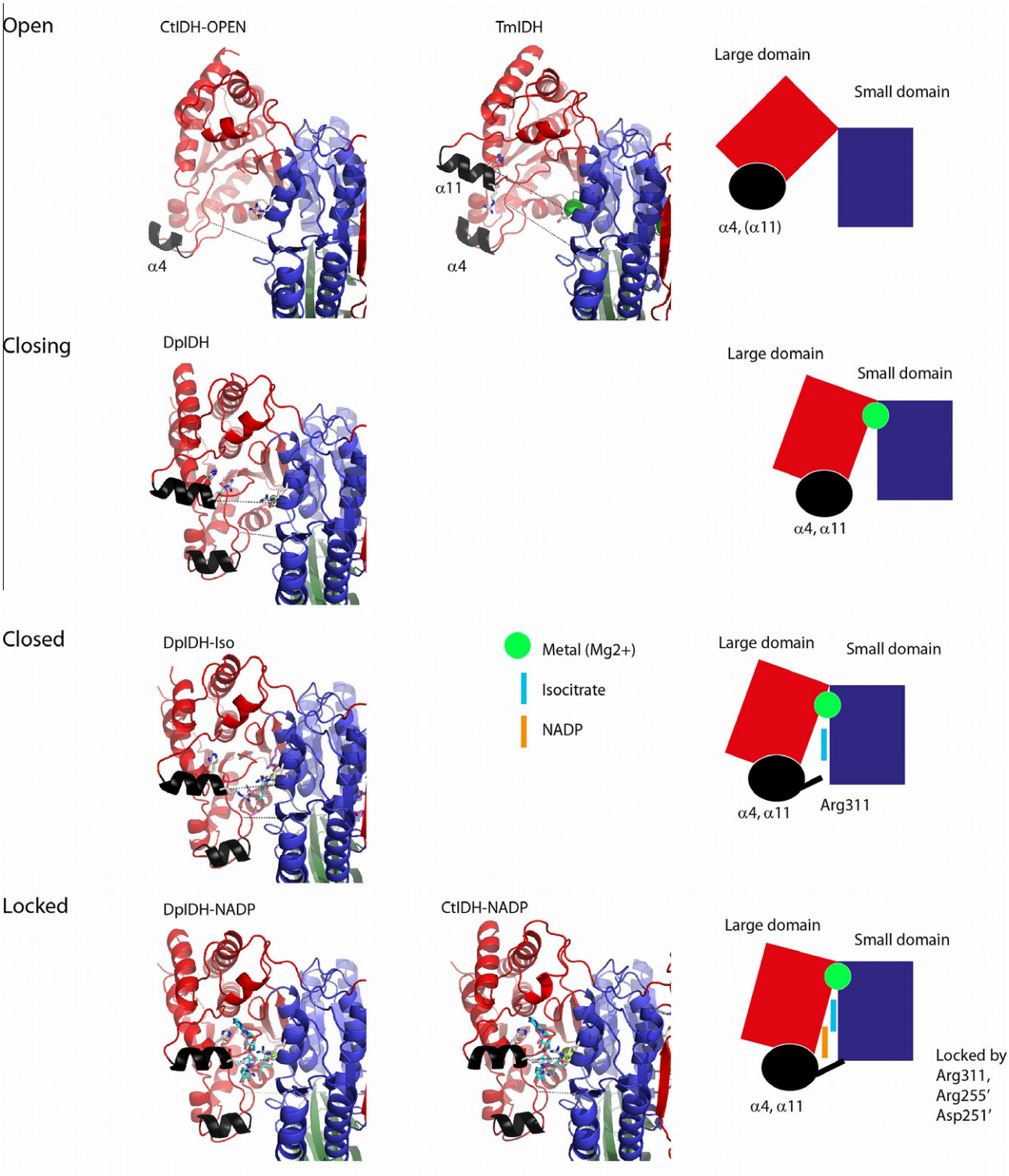

Fig. 8. The locking of the large domain onto the small domain seems unique in *Ct*IDH and *Dp*IDH starting from open (*Ct*IDH-Open, *Tm*Open), to the closing (*Dp*IDH), the closed (*Dp*IDH-Iso) to finally the locked state (*Ct*IDH–NADP, *Dp*IDH–NADP). Here helix α4 comes in place, Arg311 is important for binding the large to the small domain and finally Arg311, Asp251′ and Arg255′ make unique interactions and binding properties for $NADP^+$.

*Tm*IDH) share a high level of primary sequence identity of about 60%, and a moderate identity to eukaryotic subfamily II homologs of about 50% (*Hc*IDH, *Pc*IDH and *Sc*IDH). Even though, the secondary structure elements are however highly conserved together with the active site given by the cofactor and substrate binding residues (Fig. 4), the three dimensional structures provide the distinct differences that reveal the structural explanations to the activity-stability-flexibility relationship.

The prokaryotic *Ct*IDH and *Dp*IDH IDHs are structurally very similar to the eukaryotic subfamily II IDHs, however they display differences in cofactor interaction and locking of the active site. For that reason, we suggest a new active site locking mechanism

(Fig. 8), which consists of an open and locked *Ct*IDH structure and a closing, closed and locked structure of *Dp*IDH. These organized subtle movements in *Ct*IDH and *Dp*IDH regulate the catalytic efficiency at their operational temperature.

Acknowledgements

This work was supported by the Norwegian Research Council (Project No. 153774/420). The Norwegian Structural Biology Centre (NorStruct) is supported by the National Functional Genomics Program (FUGE), Research Council of Norway (RCN). Provision of beamtime at ID29 and SNBL at the European Synchrotron Radiation Facility (ESRF) and at BESSY, Berlin BL14.2 is gratefully acknowledged. We thank Marit Steine Madsen for skillful technical help and Thomas Jeffrey Keen for language improvements.

References

[1] Ceccarelli, C., Grodsky, N.B., Ariyaratne, N., Colman, R.F. and Bahnson, B.J. (2002) Crystal structure of porcine mitochondrial NADP$^+$-dependent isocitrate dehydrogenase complexed with Mn^{2+} and isocitrate. Insights into the enzyme mechanism. J. Biol. Chem. 277, 43454–43462.

[2] Dean, A.M. and Koshland Jr., D.E. (1993) Kinetic mechanism of *Escherichia coli* isocitrate dehydrogenase. Biochemistry 32, 9302–9309.

[3] Doyle, S.A., Fung, S.Y. and Koshland Jr., D.E. (2000) Redesigning the substrate specificity of an enzyme: isocitrate dehydrogenase. Biochemistry 39, 14348–14355.

[4] Fedøy, A.E., Yang, N., Martinez, A., Leiros, H.K. and Steen, I.H. (2007) Structural and functional properties of isocitrate dehydrogenase from the psychrophilic bacterium *Desulfotalea psychrophila* reveal a cold-active enzyme with an unusual high thermal stability. J. Mol. Biol. 372, 130–149.

[5] Huang, Y.C., Grodsky, N.B., Kim, T.K. and Colman, R.F. (2004) Ligands of the Mn^{2+} bound to porcine mitochondrial NADP-dependent isocitrate dehydrogenase, as assessed by mutagenesis. Biochemistry 43, 2821–2828.

[6] Huang, Y.C. and Colman, R.F. (2005) Location of the coenzyme binding site in the porcine mitochondrial NADP-dependent isocitrate dehydrogenase. J. Biol. Chem. 280, 30349–30353.

[7] Hurley, J.H., Dean, A.M., Koshland Jr., D.E. and Stroud, R.M. (1991) Catalytic mechanism of NADP(+)-dependent isocitrate dehydrogenase: implications from the structures of magnesium-isocitrate and NADP+ complexes. Biochemistry 30, 8671–8678.

[8] Karlstrom, M., Stokke, R., Steen, I.H., Birkeland, N.K. and Ladenstein, R. (2005) Isocitrate dehydrogenase from the hyperthermophile *Aeropyrum pernix*: X-ray structure analysis of a ternary enzyme-substrate complex and thermal stability. J. Mol. Biol. 345, 559–577.

[9] Karlstrom, M., Steen, I.H., Madern, D., Fedoy, A.E., Birkeland, N.K. and Ladenstein, R. (2006) The crystal structure of a hyperthermostable subfamily II isocitrate dehydrogenase from *Thermotoga maritima*. FEBS J. 273, 2851–2868.

[10] Kim, S.Y., Hwang, K.Y., Kim, S.H., Sung, H.C., Han, Y.S. and Cho, Y. (1999) Structural basis for cold adaptation. Sequence, biochemical properties, and crystal structure of malate dehydrogenase from a psychrophile *Aquaspirillium arcticum*. J. Biol. Chem. 274, 11761–11767.

[11] Kim, T.K., Lee, P. and Colman, R.F. (2003) Critical role of Lys212 and Tyr140 in porcine NADP-dependent isocitrate dehydrogenase. J. Biol. Chem. 278, 49323–49331.

[12] Kim, T.K. and Colman, R.F. (2005) Ser95, Asn97, and Thr78 are important for the catalytic function of porcine NADP-dependent isocitrate dehydrogenase. Protein Sci. 14, 140–147.

[13] Lee, P. and Colman, R.F. (2006) Thr(373), Asp(375), and Lys(260) are in the coenzyme site of porcine NADP-dependent isocitrate dehydrogenase. Arch. Biochem. Biophys. 450, 183–190.

[14] Singh, S.K., Matsuno, K., LaPorte, D.C. and Banaszak, L.J. (2001) Crystal structure of Bacillus subtilis isocitrate dehydrogenase at 1.55 Å. Insights into the nature of substrate specificity exhibited by *Escherichia coli* isocitrate dehydrogenase kinase/phosphatase. J. Biol. Chem. 276, 26154–26163.

[15] Steen, I.H., Madern, D., Karlstrom, M., Lien, T., Ladenstein, R. and Birkeland, N.K. (2001) Comparison of isocitrate dehydrogenase from three hyperthermophiles reveals differences in thermostability, cofactor specificity, oligomeric state, and phylogenetic affiliation. J. Biol. Chem. 276, 43924–43931.

[16] Xu, X., Zhao, J., Xu, Z., Peng, B., Huang, Q., Arnold, E. and Ding, J. (2004) Structures of human cytosolic NADP-dependent isocitrate dehydrogenase reveal a novel self-regulatory mechanism of activity. J. Biol. Chem. 279, 33946–33957.

[17] Stokke, R., Birkeland, N.K. and Steen, I.H. (2007) Thermal stability and biochemical properties of isocitrate dehydrogenase from the thermoacidophilic archaeon *Thermoplasma acidophilum*. Extremophiles 11, 397–402.

[18] Stokke, R., Karlstrom, M., Yang, N., Leiros, I., Ladenstein, R., Birkeland, N.K. and Steen, I.H. (2007) Thermal stability of isocitrate dehydrogenase from *Archaeoglobus fulgidus* studied by crystal structure analysis and engineering of chimers. Extremophiles 11, 481–493.

[19] Stokke, R., Madern, D., Fedoy, A.E., Karlsen, S., Birkeland, N.K. and Steen, I.H. (2007) Biochemical characterization of isocitrate dehydrogenase from *Methylococcus capsulatus* reveals a unique NAD+-dependent homotetrameric enzyme. Arch. Microbiol. 187, 361–370.

[20] Bolduc, J.M., Dyer, D.H., Scott, W.G., Singer, P., Sweet, R.M., Koshland Jr., D.E. and Stoddard, B.L. (1995) Mutagenesis and Laue structures of enzyme intermediates: isocitrate dehydrogenase. Science 268, 1312–1318.

[21] Dean, A.M. and Golding, G.B. (1997) Protein engineering reveals ancient adaptive replacements in isocitrate dehydrogenase. Proc Natl Acad Sci U S A 94, 3104–3109.

[22] Hurley, J.H., Chen, R. and Dean, A.M. (1996) Determinants of cofactor specificity in isocitrate dehydrogenase: structure of an engineered NADP+ → NAD+ specificity-reversal mutant. Biochemistry 35, 5670–5678.

[23] Stoddard, B.L. (1998) New results using Laue diffraction and time-resolved crystallography. Curr. Opin. Struct. Biol. 8, 612–618.

[24] Stoddard, B.L., Cohen, B.E., Brubaker, M., Mesecar, A.D. and Koshland Jr., D.E. (1998) Millisecond Laue structures of an enzyme-product complex using photocaged substrate analogs. Nat. Struct. Biol. 5, 891–897.

[25] Aktas, D.F. and Cook, P.F. (2009) A lysine-tyrosine pair carries out acid-base chemistry in the metal ion-dependent pyridine dinucleotide-linked β-hydroxyacid oxidative decarboxylases. Biochemistry 48, 3565–3577.

[26] Karshikoff, A. and Ladenstein, R. (2001) Ion pairs and the thermotolerance of proteins from hyperthermophiles: a "traffic rule" for hot roads. Trends Biochem. Sci. 26, 550–556.

[27] Vieille, C. and Zeikus, G.J. (2001) Hyperthermophilic enzymes: sources, uses, and molecular mechanisms for thermostability. Microbiol. Mol. Biol. Rev. 65, 1–43.

[28] Szilagyi, A. and Zavodszky, P. (2000) Structural differences between mesophilic, moderately thermophilic and extremely thermophilic protein subunits: results of a comprehensive survey. Structure 8, 493–504.

[29] Jaenicke, R. and Bohm, G. (1998) The stability of proteins in extreme environments. Curr. Opin. Struct. Biol. 8, 738–748.

[30] Smalås, A.O., Leiros, H.-K.S., Os, V. and Willassen, N.P. (2000) Cold adapted enzymes. Biotechnol Annu Rev 6, 1–57.

[31] Siddiqui, K.S. and Cavicchioli, R. (2006) Cold-adapted enzymes. Annu. Rev. Biochem. 75, 403–433.

[32] Peng, Y., Zhong, C., Huang, W. and Ding, J. (2008) Structural studies of *Saccharomyces cerevesiae* mitochondrial NADP-dependent isocitrate dehydrogenase in different enzymatic states reveal substantial conformational changes during the catalytic reaction. Protein Sci. 17, 1542–1554.

[33] Bradford, M.M. (1976) A rapid and sensitive method for the quantitation of microgram quantities of protein utilizing the principle of protein-dye binding. Anal. Biochem. 72, 248–254.

[34] Eisenthal, R. and Cornish-Bowden, A. (1974) The direct linear plot. A new graphical procedure for estimating enzyme kinetic parameters. Biochem J 139, 715–720.

[35] Lonhienne, T., Gerday, C. and Feller, G. (2000) Psychrophilic enzymes: revisiting the thermodynamic parameters of activation may explain local flexibility. Biochim. Biophys. Acta 1543, 1–10.

[36] Kabsch, W. (1993) Automatic processing of rotation diffraction data from crystals of initially unknown symmetry and cell constants. J Appl Crystallog 24, 795–800.

[37] Collaborative Computational Project, Number 4 (1994) The CCP4 suite: programs for protein crystallography. Acta Crystallogr. D Biol. Crystallogr. D50, 760–763.

[38] Murshudov, G.N., Vagin, A.A., Lebedev, A., Wilson, K.S. and Dodson, E.J. (1999) Efficient anisotropic refinement of macromolecular structures using FFT. Acta Crystallogr. D Biol. Crystallogr. 55, 247–255.

[39] Jones, T.A., Zou, J.Y., Cowan, S.W. and Kjeldgaard (1991) Improved methods for building protein models in electron density maps and the location of errors in these models. Acta Crystallogr. A 47 (Pt 2), 110–119.

[40] McDonald, I.K. and Thornton, J.M. (1994) Satisfying hydrogen bonding potential in proteins. J. Mol. Biol. 238, 777–793.

[41] Rocchia, W., Sridharan, S., Nicholls, A., Alexov, E., Chiabrera, A. and Honig, B. (2002) Rapid grid-based construction of the molecular surface and the use of induced surface charge to calculate reaction field energies: applications to the molecular systems and geometric objects. J. Comput. Chem. 23, 128–137.

[42] Herrero, A.A. and Gomez, R.F. (1980) Development of ethanol tolerance in *Clostridium thermocellum*: effect of growth temperature. Appl. Environ. Microbiol. 40, 571–577.

[43] Feller, G. (2010) Protein stability and enzyme activity at extreme biological temperatures. Journal of Physics-Condensed Matter 22, 323101.

[44] Marx JC, Collins T, D'Amico S, Feller G & Gerday C (2007) Cold-Adapted Enzymes from Marine Antarctic Microorganisms. Mar Biotechnol (NY).

[45] Valencia, E., Larroy, C., Ochoa, W.F., Pares, X., Fita, I. and Biosca, J.A. (2004) Apo and Holo structures of an NADPH-dependent cinnamyl alcohol dehydrogenase from *Saccharomyces cerevisiae*. J. Mol. Biol. 341, 1049–1062.

[46] Huang, Y.C. and Colman, R.F. (2002) Evaluation by mutagenesis of the roles of His309, His315, and His319 in the coenzyme site of pig heart NADP-dependent isocitrate dehydrogenase. Biochemistry 41, 5637–5643.